Dalton Transactions

ROYAL SOCIETY OF CHEMISTRY

PAPER

View Article Online
View Journal | View Issue

Cite this: *Dalton Trans.*, 2025, **54**, 15773

Wide variability in the stability of Pd_6L_x-type coordination cages

Jean de Montmollin, Farzaneh Fadaei-Tirani and Kay Severin *

The relative stability of hexanuclear Pd-based coordination cages has been investigated. For this purpose, we have synthesized eight cages of type $[Pd_6L_{12}]^{12+}$ or $[Pd_6L_8]^{12+}$. Six of these cages have been described before, and two are reported here for the first time, including crystallographic analyses. The stability of the cages was investigated by subjecting cage solutions in DMSO-d_6 or CD_3CN to different amounts of pyridine. The cage degradation was monitored by ^1H NMR. Our findings reveal significant variability in cage stability. The relative thermodynamic stability of the cages varies by nearly two orders of magnitude and the kinetic stability by more than four orders of magnitude. The stability of the cages is primarily governed by the nature of the donor group, with denticity playing a subordinate role. The high kinetic stability conferred by imidazole-based ligands provided access to a rare octanuclear cage of the type $[Pd_8L_{16}]^{16+}$, featuring a square antiprismatic geometry.

Received 16th September 2025,
Accepted 2nd October 2025

DOI: 10.1039/d5dt02223a

rsc.li/dalton

Introduction

Coordination cages based on $[Pd(N\text{-donor})_4]^{2+}$ links represent a well-established class of metallosupramolecular architectures.[1] Work in this area has primarily focused on exploring the structural diversity of these assemblies. Cages with a wide range of nuclearities have been reported, spanning from simple $[Pd_2L_4]^{4+}$-type cages[2] to giant $[Pd_{48}L_{96}]^{96+}$ nanospheres.[3] Moreover, intricate architectures such as interlocked cages[4] and heteroleptic assemblies[5] were uncovered. The self-assembly of these cages typically relies on the predictable square-planar coordination geometry of Pd^{II} centers and the careful design of N-donor ligands, which govern the size, shape, and symmetry of the resulting supramolecular architectures.[1,6]

Alongside structural investigations, significant efforts have been devoted to exploring the functional properties of Pd-based cages, including their host–guest chemistry, catalytic activity, photophysical properties, and potential for molecular separation, extraction, and delivery.[1,7–9] The use of Pd cages in materials science has also been reported.[10]

A potential Achilles heel for applications of Pd-based cages is their limited chemical stability. Cleavage of the $[Pd(N\text{-donor})_4]^{2+}$ crosslinks was observed for a range of simple anions such as chloride,[11] phosphate,[12] or acetate.[13] Biomolecules such as amino acids[11b–d] or glutathione[14] can likewise act as competitive ligands, resulting in cage disassembly. Pd cages also show limited stability under acidic conditions.[15]

As expected, the strength of the coordination bond between Pd^{2+} and the respective N-donor ligand is a crucial factor for the stability of $[Pd(N\text{-donor})_4]^{2+}$-based cages.[11c,d,15] Imidazole ligands are typically stronger donors than simple pyridine ligands.[16] Accordingly, cages based on polyimidazole ligands are expected to be more stable than cages based on polypyridyl ligands. Experimentally, this point was corroborated by ligand exchange studies.[17] 4-Dimethylaminopyridine (DMAP) is a potent ligand for Pd^{2+}, and several studies have shown that Pd-based cages are quantitatively destroyed upon addition of DMAP.[11f,18]

While the importance of the strength of the N-donor is well established, other potential factors influencing the stability of Pd-based cages are less well understood. For instance, cages constructed from tritopic ligands should be favored over those based on ditopic ligands from an entropy point of view (assuming identical nuclearity). Regarding the relative *kinetic* stability of Pd-based cages, there is only limited information available, with previous studies focusing largely on simple dinuclear $[Pd_2L_4]^{4+}$ cages.[11b–d]

For the present study, we have compared the thermodynamic and kinetic stability of eight hexanuclear Pd cages. The cages have a similar octahedral geometry, but they feature different bridging ligands, including di- and tritopic N-donors, and different types of donor groups. Our investigations have revealed a wide variability in the relative stability of the cages. Notably, the kinetic stability was found to differ by more than four orders of magnitude. We have exploited the high kinetic stability, which is provided by imidazole-based ligands, to

Institut des Sciences et Ingénierie Chimiques, École Polytechnique Fédérale de Lausanne (EPFL), 1015 Lausanne, Switzerland. E-mail: kay.severin@epfl.ch

access a rare octanuclear cage of type $[Pd_8L_{16}]^{16+}$ with a square antiprismatic structure.

Results and discussion

For our study, we have employed the di- and tritopic ligands **L1–L8** (Fig. 1). The ligands feature *N*-substituted imidazoles (**L1–L3**) or substituted pyridines (**L4–L8**) as donor groups. In addition to the pyridyl group, ligand **L5** also has a 1,2,4-triazole donor group. To the best of our knowledge, the thiophenylene-bridged ligand **L3** has so far not been used for the construction of Pd-based cages. Its synthesis was achieved by Ullman coupling (for details, see the SI).

The ligands **L1–L8** were combined with $Pd(NO_3)_2$ or $[Pd(CH_3CN)_4](BF_4)_2$ to give the hexanuclear Pd cages **C1–C8** after thermal equilibration in either DMSO-d_6 or CD_3CN (Scheme 1). The choice of the Pd precursor and the solvent was largely dictated by the solubility of the final assembly.

The known cages **C4**,[19] **C7** [19] and **C8** [20] were isolated according to literature procedure. Cage **C2** was reported to form by combining **L2** with $Pd(NO_3)_2$ in DMSO.[21] Instead, we synthesized **C2** in CD_3CN with $[Pd(CH_3CN)_4](BF_4)_2$ and purified it by precipitation with ethyl acetate. Cage solutions of **C5** and **C6** in CD_3CN were obtained without additional purification steps following literature procedures.[22,23]

The cages **C1** and **C3** have not been reported before. The commercially available ligand **L1** (4 equiv.) was combined with $[Pd(CH_3CN)_4](BF_4)_2$ (3 equiv.) in CD_3CN. After heating the mixture for 20 h to 80 °C, the ^{1}H NMR spectrum showed broad, ill-defined peaks. However, when the solution was heated to 150 °C for 20 h using a microwave reactor, the ^{1}H NMR spectrum indicated the formation of a defined assembly with high apparent symmetry (see Fig. S4). The high-resolution mass spectrum showed prominent peaks for a hexanuclear complex of the formula $[[Pd_6(\mathbf{L1})_8](BF_4)_n]^{(12-n)+}$ (n = 2–8) (see Fig. S10). Single crystals of cage **C1** were grown by slow vapor diffusion of ethyl acetate and diethyl ether into a solution of **C1** in CD_3CN. Single-crystal XRD analysis of **C1** showed the expected octahedral arrangement of the six Pd^{2+} ions (Fig. 2). With a maximum Pd···Pd distance of 25.4(2) Å, cage **C1** is the second largest cage in our cohort, only topped by **C4** (Pd···Pd = 25.6 Å). Four BF_4^- ions in crystalline **C1** are found in the cage cavity, two at the surface between ligands, and six outside the cage.

Cage **C3** was obtained by combining **L3** (2 equiv.) with $[Pd(CH_3CN)_4](BF_4)_2$ (1 equiv.) in CD_3CN. After heating to 80 °C for 20 hours, **C3** was formed in nearly quantitative yield as shown by ^{1}H NMR spectroscopy (Fig. S13). The formation of a hexanuclear cage was confirmed by mass spectrometry: dominant peaks for a complex of the formula $[[Pd_6(\mathbf{L3})_{12}](BF_4)_n]^{(12-n)+}$ (n = 4–9) were observed (Fig. S19). Single crystals of cage **C3** were grown by slow vapor diffusion of diisopropyl ether into a solution of **C3** in CD_3CN. Single-crystal XRD analysis of **C3** showed the expected octahedral arrangement of the six Pd^{2+} ions (Fig. 2). The maximum Pd···Pd distance of **C3** is 16.6(1) Å, which makes **C3** the smallest cage that we have used in our study. Four BF_4^- ions in crystalline **C3** are found inside the cage, and eight could be localized outside. In solution, there is apparently a rapid exchange between the BF_4^- ions as only one ^{19}F NMR signal was observed.

It is interesting to note that the ligands **L2** and **L3** give both octahedral coordination cages, despite the fact that the two

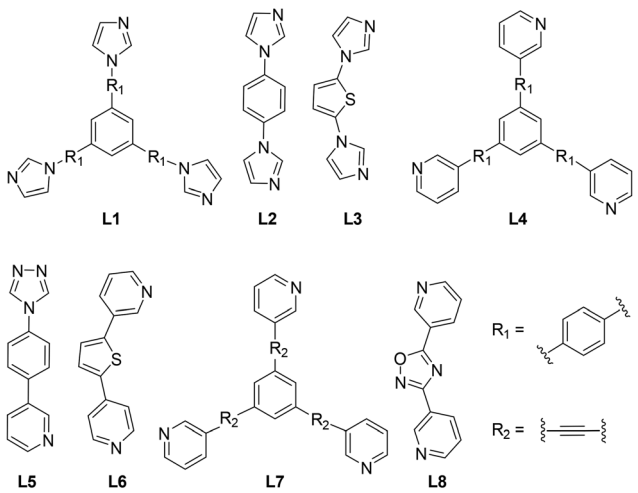

Fig. 1 Structures of the ligands **L1–L8**.

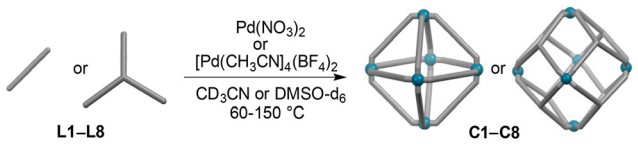

Scheme 1 Synthesis of the hexanuclear coordination cages **C1–C8**.

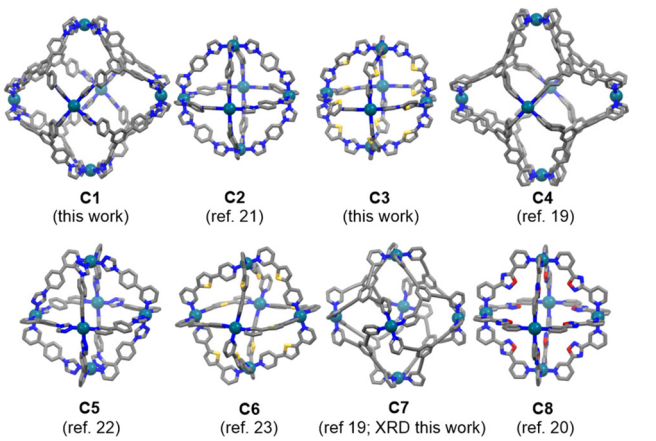

Fig. 2 Molecular structures of the cages **C1–C8** in the solid state, as determined by single-crystal XRD. Hydrogen atoms and counter anions are omitted. Color coding: Pd dark green, C grey, N blue, O red. The data for the known cages **C2**, **C4**, **C5**, **C6**, and **C8** were taken from the literature.

ligands have distinct spacers (phenylene *vs.* thiophenylene). However, the ligand bent angle, as defined by the angle between the coordinate vectors of the two N-donor groups, is not fixed in these ligands (the bent angle changes upon rotation around the spacer–imidazole bond). In **C3**, the central thiophenylene spacers are rotated out of plane relative to the coplanar imidazole moieties, thereby increasing the bent angle and enabling an octahedral arrangement.

The synthesis of cage **C7** was reported by Crowley and co-workers.[19] They were unable to obtain XRD-quality single crystals, and molecular modeling was used to derive structural information. We could obtain single crystals of **C7** in a similar fashion as for **C3**, *i.e.* by slow vapor diffusion of diisopropyl ether into a solution of **C7** in CD_3CN. Unlike in the molecular model reported by Crowley *et al.*,[19] the pyridyl donor groups in crystalline **C7** adopt a propeller-like conformation around each palladium center. The six Pd(pyridyl)$_4$ complexes in **C7** show the same helicity, giving rise to pairs of enantiomeric cages in the solid state (see Fig. S58).

To quantify the relative stability of the cages **C1–C8**, we introduce DPy_{50} ('*Destructive Pyridine*') values. In analogy to the commonly used LD_{50} values to quantify the toxicity of compounds, the DPy_{50} value gives the amount of pyridine (in cage equivalents) at which 50% of the cage is destroyed at thermodynamic equilibrium, given a uniform initial cage concentration.

The DPy_{50} values for the cages **C1–C8** were determined as follows: solutions of the cages (~0.33 mM) were subjected to increasing amounts of pyridine-d_5 (Scheme 2). Either DMSO-d_6 or CD_3CN was used as the solvent, with the choice being influenced by the solubility of the respective cage. After each pyridine addition, the NMR tube was heated for 2 h at 80 °C. This thermal treatment was found to be sufficient to establish the new thermodynamic equilibrium (see Fig. S27). Subsequently, a ^{1}H NMR spectrum was recorded, and the decrease in cage concentration was quantified using durene as an internal standard.

The NMR spectra recorded after the addition of pyridine-d_5 were remarkably 'clean'. The major signals in the spectra could be assigned to those of the free ligands and of the remaining cages. The Pd^{2+} ions from the destroyed cages were captured in the form of $[Pd(pyridine\text{-}d_5)_4]^{2+}$, as confirmed by mass spectrometry. Only minor amounts of other, unidentified species were observed. As a representative example, selected ^{1}H NMR spectra for the decomposition of **C1** are depicted in Fig. 3.

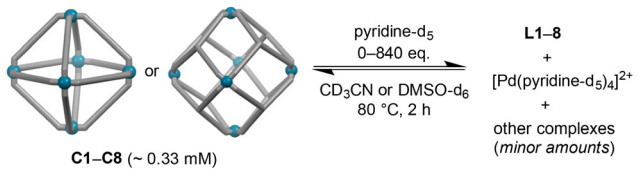

Scheme 2 Destruction of the cages **C1–C8** with pyridine-d_5.

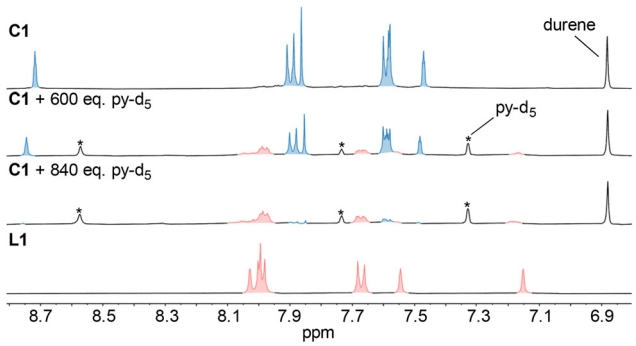

Fig. 3 Aromatic parts of the ^{1}H NMR spectra (CD_3CN, 400 MHz) of **C1**, **C1** after equilibration with 600 eq. of pyridine-d_5, **C1** after equilibration with 840 eq. of pyridine-d_5, and the 'free' ligand **L1** (from the top to the bottom).

From the NMR spectra, we were able to derive the cage concentrations at a given pyridine-d_5 concentration. The DPy_{50} values were obtained from the intersection between the linear interpolation of the data points and the horizontal line corresponding to 50% cage decomposition (Fig. 4a). Since all cages are converted largely into the same complex, $[Pd(pyridine\text{-}d_5)_4]^{2+}$, the DPy_{50} values serve as a proxy for the relative thermodynamic stability of the cages.

In CD_3CN, both the most stable cage, **C1** (DPy_{50} = 624), and the least stable cage, **C7** (DPy_{50} = 10), are based on tritopic ligands (Fig. 4b). Apparently, the nature of the donor group is more important than ligand denticity. The high stability of the cages **C2** (DPy_{50} = 534) and **C3** (DPy_{50} = 165) with ligands featuring strong imidazole donors further underlines this point. The drop in stability between **C2** and **C3** can be attributed, at least in part, to the electronic effect of the spacer group. Calculations show that 1-phenylimidazole is slightly more

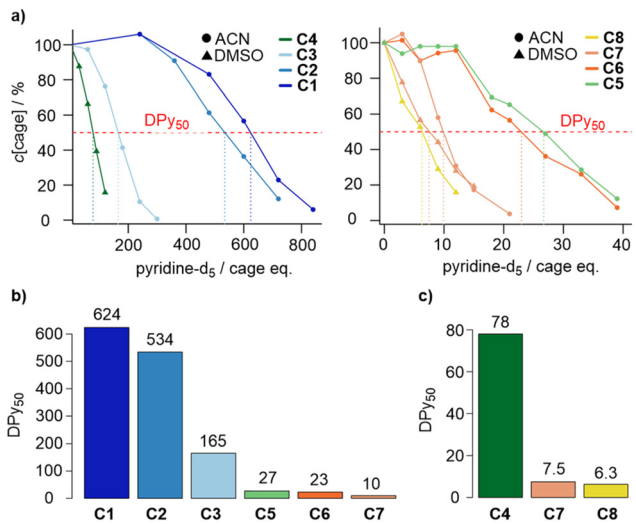

Fig. 4 Destruction of the cages **C1–C8** upon addition of increasing amounts of pyridine-d_5 (a). The resulting DPy_{50} values for experiments performed in CD_3CN (b) or in DMSO-d_6 (c).

basic than 1-thiophenylimidazole (for details, see Fig. S26). Accordingly, it is expected that **L2** is a better donor than **L3**.

For the values determined in DMSO-d_6 (Fig. 4c), a pronounced difference in the stability of the $[Pd_6L_8]^{12+}$ cages **C4** (DPy_{50} = 78) and **C7** (DPy_{50} = 7.5) was observed. As in the case of **C2** and **C3**, we attribute this difference to the electronic effect of the spacer (alkynyl *vs.* phenylene). For cage **C7**, we were able to perform experiments in both CD_3CN and DMSO-d_6, yielding similar values in both solvents.

The lowest thermodynamic stability of all cages was found for **C8**. The poor stability is likely linked to the low basicity of the pyridine donors in this ligand (for details, see Fig. S26).

To evaluate the kinetic stability of the cages **C1–C8**, we added a large excess of pyridine-d_5 to solutions of the cages in CD_3CN or DMSO-d_6 (~0.33 mM). The cage degradation with time under these pseudo first-order kinetics conditions was then monitored by ^{1}H NMR spectroscopy. The amount of pyridine-d_5 was chosen so that cage disassembly occurred on the minute-to-hour time scale.

It quickly became apparent that we could not use a uniform amount of pyridine-d_5 for these experiments because the kinetic stability of the cages varied too much. Therefore, we decided to evaluate the relative stability of the cages in pairs. For a given pair, a fixed amount of pyridine-d_5 was employed, and the half-lives ($t_{1/2}$) of the decomposition reactions were determined by linear regression. For the cage pair **C1**/**C2**, for example, 3000 equivalents of pyridine-d_5 were used, leading to the nearly complete disassembly of both cages within 20–30 min (Fig. 5). From the time-dependent NMR measurements, we were able to derive $t_{1/2}$ values of 3.3 min (**C1**) and 10 min (**C2**).

For experiments in CD_3CN, we have analyzed the relative kinetic stability of the cage pairs **C7**/**C6** (120 eq. pyridine), **C6**/**C5** (240 eq. pyridine), **C5**/**C3** (1200 eq. pyridine), **C3**/**C1** (1200 eq. pyridine), and **C2**/**C1** (3000 eq. pyridine) (Fig. 6a). For the comparison of **C3** with **C5**, we observed the complete destruction of **C5** within the time required to record the first ^{1}H NMR spectrum (<1 min). Although lowering the pyridine-d_5 concentration slowed the disassembly of **C5**, it also disrupted the pseudo-first-order kinetics for **C3**. Therefore, we performed a standard kinetic analysis for **C3** with 1200 equivalents of pyridine-d_5 ($t_{1/2}$ = 15 min), and we estimated the half-life of **C5** to be 0.3 min or shorter.

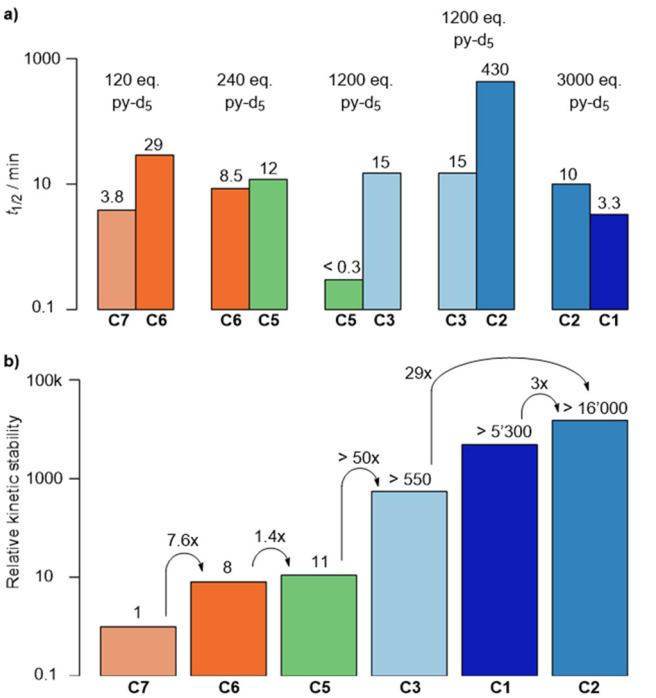

Fig. 6 Half-lives of the decomposition reaction of the cages **C1**, **C2**, **C3**, **C5**, **C6**, and **C7** in CD_3CN upon addition of variable amounts of pyridine-d_5 (a), and the relative kinetic stability of the cages (b).

By analyzing these cage pairs, we were able to rank the cages in terms of kinetic stability and express their stability relative to that of **C7**, which exhibited the lowest stability. We estimate that **C2** is at least 16 000 times more stable than **C7** (Fig. 6b). It should be noted, however, that these values are approximate, as error accumulates with each multiplication step.

As in the thermodynamic analysis, the kinetic stability of the cages **C4** and **C8** was investigated in DMSO-d_6, due to their limited solubility in CD_3CN. Cage **C7**, which is soluble in both solvents, was included for comparison. The cages were analyzed again in pairs, with 120 equivalents of pyridine-d_5 used for **C7**/**C8**, and 600 equivalents of pyridine-d_5 used for **C4**/**C8** (Fig. 7a). The results showed that **C8** is 11 times more stable than **C7**, and that **C4** is 17 times more stable than **C8** (Fig. 7b).

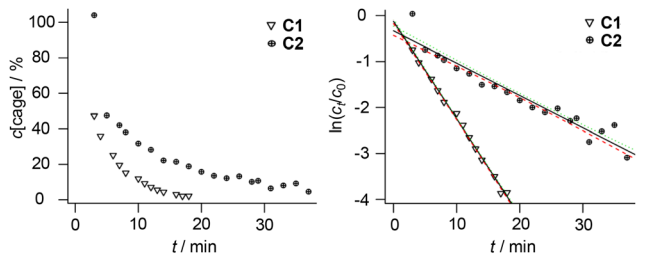

Fig. 5 Time course for the disassembly of the cages **C1** and **C2** after the addition of 3000 equivalents of pyridine-d_5 (left) and the corresponding linear regression assuming first-order kinetics (right).

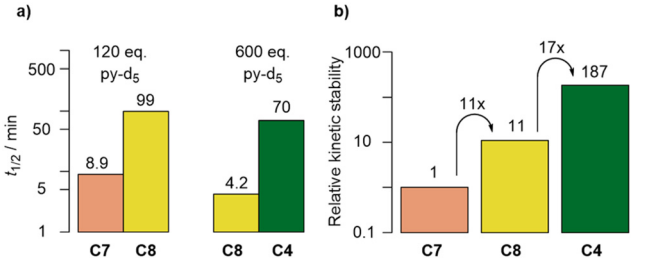

Fig. 7 Half-lives of the decomposition reaction of the cages **C4**, **C7**, and **C8** in DMSO-d_6 upon addition of 120 or 600 equivalents of pyridine-d_5 (a), and the relative kinetic stability of the cages (b).

Since cage **C7** was studied in both, CD_3CN and DMSO-d_6, we were able to evaluate the solvent effect on the kinetic stability. The decay of **C7** was found to be approximately twice as fast in CD_3CN ($t_{1/2}$ = 3.8 min) when compared to DMSO-d_6 ($t_{1/2}$ = 8.9 min).

Overall, the ranking of the cages in terms of kinetic stability (Fig. 6 and 7) aligns well with their relative thermodynamic stability (Fig. 4). In CD_3CN, only the ranking of the cages **C1** and **C2** is reversed, whereas in DMSO-d_6, the ranking of the cages **C7** and **C8** is inverted. However, the differences in these cases are not pronounced. In terms of stability, the imidazole-based palladium cages **C1–C3** stand out, surpassing the other five cages by a large margin.

In the following, we show that the kinetic stability of assemblies with the imidazole ligand **L2** can be used to access a rare $[Pd_8L_{16}]^{16+}$-type cage. When trying to synthesize cage **C2** in deuterated nitromethane (80 °C, 20 h) instead of CD_3CN, we noted the presence of side products (Fig. 8a). The mass spectrum of the reaction mixture indicated that the larger cages $[Pd_8(\mathbf{L2})_{16}]^{16+}$ and $[Pd_9(\mathbf{L2})_{18}]^{18+}$ had formed along with the expected hexanuclear cage $[Pd_6(\mathbf{L2})_{12}]^{12+}$ (Fig. 8b).

Octanuclear cages of type $[Pd_8L_{16}]^{16+}$ are expected to display D_{4d} symmetry, with a two-fold splitting of the NMR signals for the ligand.[24] Cages of type $[Pd_9L_{18}]^{18+}$ should show D_{3h} symmetry, with three sets of NMR signals for the donor groups.[24] Based on these symmetry considerations, we were able to

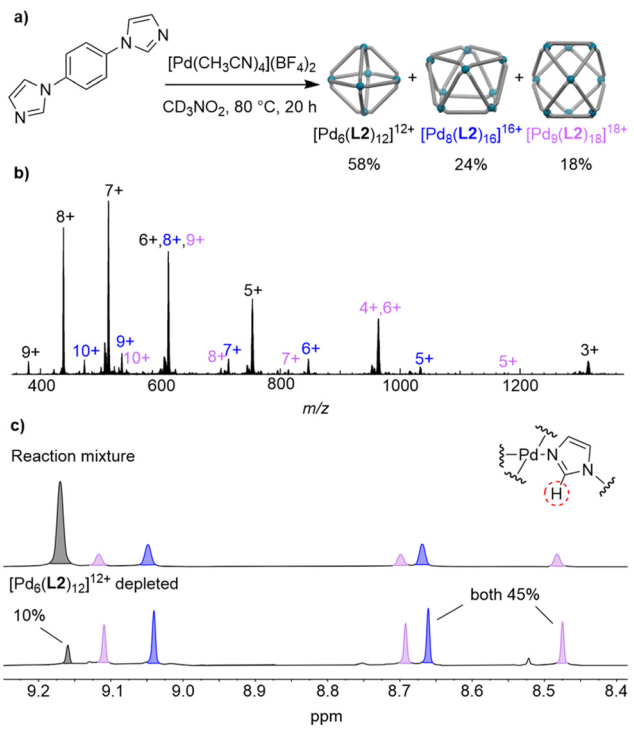

Fig. 8 (a) The reaction of **L2** with $[Pd(CH_3CN)_4](BF_4)_2$ in CD_3NO_2 gives a mixture of three cages. (b) High-resolution ESI mass spectrum of the reaction mixture. (c) Part of the ^{1}H NMR spectrum of the reaction mixture (top) and after depletion of $[Pd_6(\mathbf{L2})_{12}]^{12+}$ by precipitation with ethyl acetate (bottom). The signals originate from the proton circled in red.

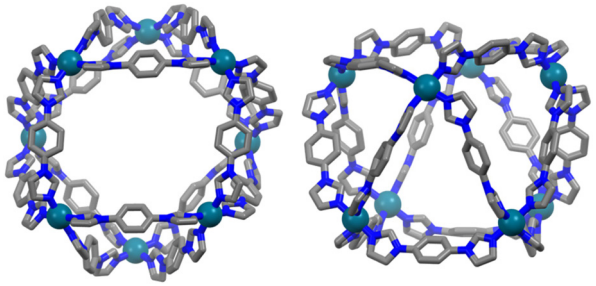

Fig. 9 Two views of the molecular structure of $[Pd_8(\mathbf{L2})_{16}]^{16+}$, as determined by single-crystal XRD. The BF_4^- anions were not located and hydrogen atoms are not shown. Color coding: Pd dark green, C grey, N blue.

deduce that the larger cages $[Pd_8(\mathbf{L2})_{16}]^{16+}$ and $[Pd_9(\mathbf{L2})_{18}]^{18+}$ had formed in 24% and 18%, respectively (Fig. 8a and c).

For Pd-based cages, the isolation of side products is often complicated by the dynamic behavior of these assemblies, which are prone to structural rearrangements. This difficulty is illustrated by an earlier report about a $[Pd_8L_{16}]^{16+}$ cage by Fujita. They had obtained spectroscopic evidence (NMR, MS) for such an octanuclear cage during the synthesis of a dodecanuclear $[Pd_{12}L_{24}]^{24+}$ cage.[24] However, the octanuclear cage rearranged into the thermodynamically more stable dodecanuclear cage upon gentle heating (60 °C, 1 h).

In contrast, no post-synthetic rearrangement was observed for the cages based on **C2**. Selective precipitation of $[Pd_6(\mathbf{L2})_{12}]^{12+}$ cage was achieved by adding ethyl acetate to the reaction mixture. After two cycles of precipitation, $[Pd_6(\mathbf{L2})_{12}]^{12+}$ accounted for only 10% of the mixture, the rest being $[Pd_8(\mathbf{L2})_{16}]^{16+}$ and $[Pd_9(\mathbf{L2})_{18}]^{18+}$ in equal amounts. The high kinetic stability of the latter cages is illustrated by the fact that the composition of the mixture was not affected by heating for 20 h at 80 °C (Fig. S25).

While we were not able to isolate $[Pd_8L_{16}]^{16+}$ on a preparative scale, we could grow crystals of this cage by slow vapor diffusion of diisopropyl ether into the $[Pd_6(\mathbf{L2})_{12}]^{12+}$-depleted solution in nitromethane. A crystallographic analysis revealed a square antiprismatic geometry for $[Pd_8(\mathbf{L2})_{16}]^{16+}$ (Fig. 9), as predicted theoretically.[24] Unfortunately, BF_4^- anions and co-crystallized solvent molecules could not be localized (see the SI for details about the data treatment). However, the connectivity could clearly be established, with a maximum Pd···Pd distance of 20.2(2) Å.

Until recently, square antiprismatic cages of type $[Pd_8L_{16}]^{16+}$ had not been characterized crystallographically. While our work was in progress, a report by Pilgrim appeared, describing the structure of a $[Pd_8L_{16}]^{16+}$ cage based on a bis-imidazole donor ligand with a perfluorobiphenyl linker.[25] The presence of fluorine atoms on the biphenyl spacer was found to be crucial for the synthesis of this octanuclear assembly.

Conclusions

The stability of cages based on $[Pd(N\text{-donor})_4]^{2+}$ links is a key factor for their potential applications. However, current knowl-

edge of the relative stability of Pd-based cages remains limited, with most prior studies focusing on simple dinuclear systems. In this work, we examined the stability of eight hexanuclear cages of the type $[Pd_6L_{12}]^{12+}$ or $[Pd_6L_8]^{12+}$. Our results reveal substantial differences in the stability of the cages. The thermodynamic stability varies by almost two orders of magnitude, while kinetic stability spans over four orders of magnitude. The primary determinant influencing cage stability is the nature of the donor group, with denticity having a lesser effect. The use of imidazole-based ligands, which impart high kinetic stability, enabled access to a rare octanuclear cage, $[Pd_8(\mathbf{L2})_{16}]^{16+}$, characterized by a square antiprismatic geometry.

Author contributions

J. d. M. performed the experiments and analyzed the data, F. F.-T. collected and processed the X-ray data, and J. d. M. and K. S. co-wrote the manuscript. All authors discussed the results and commented on the manuscript.

Conflicts of interest

There are no conflicts to declare.

Data availability

The data supporting this article have been included as part of the supplementary information (SI). Supplementary information: synthetic procedures and experimental details. See DOI: https://doi.org/10.1039/d5dt02223a.

CCDC 2487791 (**C1**), 2487789 (**C3**), 2487790 (**C7**) and 2487788 ($[Pd_8(\mathbf{L2})_{16}](BF_4)_{16}$) contain the supplementary crystallographic data for this paper.[26a–d]

Acknowledgements

The work was supported by the école Polytechnique Fédérale de Lausanne (EPFL). We thank Dr D. Ortiz (EPFL) for MS analyses, P. Gorrea-Acín (EPFL) for the synthesis of ligand **L2** and Dr R.-J. Li (EPFL) for providing **L6**.

References

1 (*a*) C. J. T. Cox, J. Hale, P. Molinska and J. E. M. Lewis, *Chem. Soc. Rev.*, 2024, **53**, 10380–10408; (*b*) T. Tateishi, M. Yoshimura, S. Tokuda, F. Matsuda, D. Fujita and S. Furukawa, *Coord. Chem. Rev.*, 2022, **467**, 214612; (*c*) J. E. M. Lewis, *Chem. Commun.*, 2022, **58**, 13873–13886; (*d*) N. B. Debata, D. Tripathy and H. S. Sahoo, *Coord. Chem. Rev.*, 2019, **387**, 273–298; (*e*) K. Harris, D. Fujita and M. Fujita, *Chem. Commun.*, 2013, **49**, 6703–6712.

2 M. Han, D. M. Engelhard and G. H. Clever, *Chem. Soc. Rev.*, 2014, **43**, 1848–1860.

3 D. Fujita, Y. Ueda, S. Sato, N. Mizuno, T. Kumasaka and M. Fujita, *Nature*, 2016, **540**, 563–566.

4 M. Frank, M. D. Johnstone and G. H. Clever, *Chem. – Eur. J.*, 2016, **22**, 14104–14125.

5 (*a*) L. Neukirch and G. H. Clever, *Chem. Sci.*, 2025, **16**, 12242–12276; (*b*) Z. T. Avery, J. L. Algar and D. Preston, *Trends Chem.*, 2024, **6**, 352–364; (*c*) C.-B. Tian and Q.-F. Sun, *Chem. – Eur. J.*, 2023, **29**, e202300195; (*d*) S. Pullen, J. Tessarolo and G. H. Clever, *Chem. Sci.*, 2021, **12**, 7269–7293; D. Bardhan and D. K. Chand, *Chem. – Eur. J.*, 2019, **25**, 12241–12269.

6 S. Saha, I. Regeni and G. H. Clever, *Coord. Chem. Rev.*, 2018, **374**, 1–14.

7 For reviews about application in catalysis, see: (*a*) Z. Ashbridge and J. N. H. Reek, *Nat. Synth.*, 2024, **3**, 1197–1207; (*b*) T. K. Piskorz, V. Marti-Centelles, R. L. Spicer, F. Duarte and P. J. Lusby, *Chem. Sci.*, 2023, **14**, 11300–11331; (*c*) M. Otte, *Eur. J. Org. Chem.*, 2023, e202300012; (*d*) A. C. Pearcy and J. D. Crowley, *Chem. – Eur. J.*, 2023, **29**, e202203752; (*e*) R. Saha, B. Mondal and P. S. Mukherjee, *Chem. Rev.*, 2022, **122**, 12244–12307; (*f*) Y. Xue, X. Hang, J. Ding, B. Li, R. Zhu, H. Pang and Q. Xu, *Coord. Chem. Rev.*, 2021, **430**, 213656; (*g*) A. B. Grommet, M. Feller and R. Klajn, *Nat. Nanotechnol.*, 2020, **15**, 256–271.

8 For reviews about applications in medicinal chemistry, see: (*a*) G. Moreno-Alcántar, M. Drexler and A. Casini, *Nat. Rev. Chem.*, 2024, **8**, 893–914; (*b*) G. Moreno-Alcántar and A. Casini, *FEBS Lett.*, 2023, **597**, 191–202.

9 For reviews about cages with interesting photophysical properties, see: (*a*) E. Benchimol, J. Tessarolo and G. H. Clever, *Nat. Chem.*, 2024, **16**, 13–21; (*b*) R. Ham, C. J. Nielsen, S. Pullen and J. N. H. Reek, *Chem. Rev.*, 2023, **123**, 5525–5261; (*c*) A. Brzechwa-Chodzyńska, W. Drożdż, J. Harrowfield and A. R. Stefankiewicz, *Coord. Chem. Rev.*, 2021, **434**, 213820; (*d*) H.-Y. Lin, L.-Y. Zhou and L. Xu, *Chem. – Asian J.*, 2021, **16**, 3805–3816.

10 For recent examples, see: (*a*) C. Hu, D. W. Chen, S. Sudan and K. Severin, *Chem. Sci.*, 2025, **16**, 5559–5564; (*b*) S. Bera, A. Dutta and P. Dastidar, *Chem. – Asian J.*, 2024, **19**, e202400419; (*c*) D. J. Lundberg, C. M. Brown, E. O. Bobylev, N. J. Oldenhuis, Y. S. Alfaraj, J. Zhao, I. Kevlishvili, H. J. Kulik and J. A. Johnson, *Nat. Commun.*, 2024, **15**, 3951; (*d*) C. Hu and K. Severin, *Angew. Chem., Int. Ed.*, 2024, **63**, e202403834; (*e*) J. Zhao, E. O. Bobylev, D. J. Lundberg, N. J. Oldenhuis, H. Wang, I. Kevlishvili, S. L. Craig, H. J. Kulik, X. Li and J. A. Johnson, *J. Am. Chem. Soc.*, 2023, **145**, 21879–21885.

11 (*a*) M. Drexler, I. Kanavos, D. Krauss, G. Moreno-Alcántar, L. M. Smith, M. E. George, T. H. Witney, R. Lobinski, L. Rong and A. Casini, *Inorg. Chem. Front.*, 2025, DOI: 10.1039/D5QI01092F; (*b*) R. A. S. Vasdev, L. F. Gaudin, D. Preston, J. P. Jogy, G. I. Giles and J. D. Crowley, *Front. Chem.*, 2018, **6**, 563; (*c*) D. Preston, S. M. McNeill,

J. E. M. Lewis, G. I. Giles and J. D. Crowley, *Dalton Trans.*, 2016, **45**, 8050–8060; (*d*) S. M. McNeill, D. Preston, J. E. M. Lewis, A. Robert, K. Knerr-Rupp, D. O. Graham, J. R. Wright, G. I. Giles and J. D. Crowley, *Dalton Trans.*, 2015, **44**, 11129–11136; (*e*) D. Preston, A. Fox-Charles, W. K. C. Lo and J. D. Crowley, *Chem. Commun.*, 2015, **43**, 9042–9045; (*f*) J. E. M. Lewis, E. L. Gavey, S. A. Cameron and J. D. Crowley, *Chem. Sci.*, 2012, **3**, 778–784.

12 G. Montà-González, D. Bastante-Rodríguez, A. Garcia-Farnández, P. J. Lusby, R. Martínez-Máñez and V. Martí-Centelles, *Chem. Sci.*, 2024, **15**, 10010–10017.

13 X.-Z. Wang, D. W. Chen, F. Fadaei-Tirani, X.-P. Zhou and K. Severin, *Angew. Chem., Int. Ed.*, 2025, **64**, e202504880.

14 (*a*) B. Aikman, R. Bonsignore, B. Woods, D. Doellerer, R. Scotti, C. Schmidt, A. A. Heidecker, A. Pöthig, E. J. Sayers, A. T. Jones and A. Casini, *Dalton Trans.*, 2022, **51**, 7476–7490; (*b*) B. Woods, D. Döllerer, B. Aikman, M. N. Wenzel, E. Sayers, F. E. Kühn, A. Jones and A. Casini, *J. Inorg. Biochem.*, 2019, **199**, 110781; (*c*) A. Ahmedova, R. Mihaylova, D. Momekova, P. Shestakova, S. Stoykova, J. Zaharieva, M. Yamashina, G. Momekov, M. Akita and M. Yoshizawa, *Dalton Trans.*, 2016, **45**, 13214–13221.

15 (*a*) R.-J. Li, C. Pezzato, C. Berton and K. Severin, *Chem. Sci.*, 2021, **12**, 4981–4984; (*b*) S. M. Jansze and K. Severin, *J. Am. Chem. Soc.*, 2019, **141**, 815–819; (*c*) S. M. Jansze, G. Cecot and K. Severin, *Chem. Sci.*, 2018, **9**, 4253–4257.

16 H. V. Huynh, *Chem. Lett.*, 2021, **50**, 1831–1841.

17 D. Samanta and P. S. Mukherjee, *Chem. – Eur. J.*, 2014, **20**, 12483–12492.

18 (*a*) V. Sivalingam, M. Parbin, S. Krishnaswamy and D. K. Chand, *Angew. Chem., Int. Ed.*, 2024, **63**, 2303403711; (*b*) A. C. Pearcy, L. S. Lisboa, D. Preston, N. B. Page, T. Lawrence, L. J. Wright, C. C. Hartinger and J. D. Crowely, *Chem. Sci.*, 2023, **14**, 8615–8623; (*c*) L. S. Lisboa, J. A. Findlay, L. J. Wright, C. G. Hartinger and J. D. Crowley, *Angew. Chem., Int. Ed.*, 2020, **59**, 11101–11107; (*d*) S. Ganta and D. K. Chand, *Inorg. Chem.*, 2018, **57**, 3624–3645; (*e*) J. J. Henkelis, J. Fisher, S. L. Warriner and M. J. Hardie, *Chem. – Eur. J.*, 2014, **20**, 4117–4125.

19 T. Y. Kim, L. Digal, M. G. Gardiner, N. T. Lucas and J. D. Crowley, *Chem. – Eur. J.*, 2017, **23**, 15089–15097.

20 K. C. Naik, S. J. Panda, A. K. Sutar and H. S. Sahoo, *Inorg. Chem. Commun.*, 2023, **158**, 111468.

21 B. Roy, R. Saha, A. K. Ghosh, Y. Patil and P. S. Mukherjee, *Inorg. Chem.*, 2017, **56**, 3579–3588.

22 J. de Montmollin, A. B. Solea, D. W. Chen, F. Fadaei-Tirani and K. Severin, *Inorg. Chem.*, 2024, **63**, 4583–4588.

23 R.-J. Li, A. Marcus, F. Fadaei-Tirani and K. Severin, *Chem. Commun.*, 2021, **57**, 10023–10026.

24 D. Fujita, H. Yokoyama, Y. Ueda, S. Sato and M. Fujita, *Angew. Chem., Int. Ed.*, 2015, **54**, 155–158.

25 S. Bhattacharyya, S. P. Argent and B. S. Pilgrim, *J. Am. Chem. Soc.*, 2025, **147**, 30296–30303.

26 (*a*) CCDC 2487791: Experimental Crystal Structure Determination, 2025, DOI: **10.5517/ccdc.csd.cc2phrb9**; (*b*) CCDC 2487789: Experimental Crystal Structure Determination, 2025, DOI: **10.5517/ccdc.csd.cc2phr87**; (*c*) CCDC 2487790: Experimental Crystal Structure Determination, 2025, DOI: **10.5517/ccdc.csd.cc2phr98**; (*d*) CCDC 2487788: Experimental Crystal Structure Determination, 2025, DOI: **10.5517/ccdc.csd.cc2phr76**.